Journal of Manufacturing Processes 131 (2024) 2255–2262

Contents lists available at ScienceDirect

Journal of Manufacturing Processes

journal homepage: www.elsevier.com/locate/manpro

Suppression of melt flow instabilities by amplifying high-frequency melt waves in laser fusion cutting

M. de Oliveira Lopes [a,*], F. Schneider [b], A. Gillner [a,b], C. Häfner [a,b]

[a] Chair for Laser Technology LLT, RWTH Aachen University, Steinbachstr. 15, 52074 Aachen, Germany
[b] Fraunhofer Institute for Laser Technology ILT, Steinbachstr. 15, 52074 Aachen, Germany

ARTICLE INFO

Keywords:
Laser cutting
Gas flow
Acoustic resonance
Nozzle design
Melt flow
Surface roughness

ABSTRACT

High-frequency resonant melt waves locally increase the stability of melt flow and enhance cut flank quality. To amplify these waves along the melt flow, an acoustically tuned cutting nozzle, termed the cutting whistle, generates gas flow oscillations based on a resonant cavity. The nozzle cavity is designed for 6 mm thick sheets, causing the gas flow to oscillate at 15 kHz within the kerf, creating a uniform melt flow with synchronized oscillating melt waves. Performance evaluations on stainless steel sheets show that, compared to a standard conical nozzle, the cutting whistle reduces surface roughness across the entire cutting depth and prevents coarse structures near the upper sheet surface and at the bottom in burr-free cuts.

1. Introduction

Laser fusion cutting using laser systems with a wavelength of 1 µm has developed into an established manufacturing process and has dominated the global market in the laser industry in recent years [1]. Despite its widespread adoption, the cutting quality of medium and thick sheet metals often falls short of industry standards, necessitating either rework or alternative methods. The primary quality concerns are the formation of bottom edge burrs and the roughness of the cut flanks caused by striation patterns. These features, especially burrs, not only diminish the aesthetic quality but also limit the technical usability of the workpiece, prompting a need for solutions that enhance the surface finish and overall cut quality.

Conventionally, an assist gas is combined coaxially with the laser beam using a conical nozzle to form a supersonic jet. This jet's primary function is to couple and transfer its momentum to the molten material, propelling it out of the kerf [2]. The force exerted by the gas plays a central role in the hydrodynamics developed on the cutting front and consequently influences the formation of striations on the cut flanks [3]. According to a model proposed in [4], due to surface tension, the molten material accumulates on the cutting front until a threshold value is reached at which the surface tension is exceeded by the driving forces of the gas flow. Therefore, the balance between gas force and resistant surface tension governs the melt flow instabilities responsible for the formation of the striations.

Experimental research using high-speed videography has explored the dependencies of melt flow dynamics on various parameters, uncovering significant effects associated with this balance. One such effect is the formation of melt strings and dry areas in the melt flow, contributing to coarser surface structures [5,6]. These instabilities, even if formed at small cutting depths, also affect larger cutting depths by causing uneven multiple reflections throughout the melt flow [7,8]. It has been shown that increasing the velocity of the waves in the melt flow by optimizing the process parameters can mitigate this problem to a certain extent [9]. In a subsequent study, it was identified that regardless of the process parameters, the lowest roughness on cut flanks occurs where melt flow exhibits high-frequency waves around 30 kHz, which is attributed to acoustic resonances in the kerf channel [10].

Based on these findings, it was hypothesized that an oscillating gas flow in the kerf could increase the frictional forces on the melt film, counteracting the surface tension and thus reducing the surface roughness. To amplify this effect, a nozzle was developed based on a resonant cavity at the far end of the nozzle close to the workpiece, the so-called cutting whistle [11]. The cutting whistle generates a pronounced gas flow oscillation, the frequency of which is determined by the cavity geometry. Experiments to evaluate the performance of the cutting whistle compared to a standard conical nozzle have shown that the average surface roughness of the cutting flanks is reduced by up to 50 %, despite using a lower flow rate. This demonstrates the great potential of this approach for improving the quality of the cut flanks while reducing

* Corresponding author.
E-mail address: marcelo.lopes@llt.rwth-aachen.de (M. de Oliveira Lopes).

https://doi.org/10.1016/j.jmapro.2024.10.040
Received 29 July 2024; Received in revised form 27 September 2024; Accepted 17 October 2024
Available online 22 October 2024

gas consumption. However, due to the limited coupling of the gas flow oscillations with the melt in the lower areas, this improvement has so far been restricted to the upper third of the cut flank.

This study aims to evaluate a new cutting whistle's design to maximize its effectiveness across the entire melt flow. Key areas of focus include the relationship between standoff distance and gas flow oscillations, and their impact on melt flow stability and surface quality. It will specifically address how gas flow oscillations affect melt flow, how the oscillatory behavior of the gas flow can be enhanced to improve melt flow also in the lower cutting front, and how effective and consistent the cutting whistle is in coupling gas flow oscillations with melt flow across different standoff distances. By addressing these questions, the study aims to provide meaningful insights that could lead to advancements in laser cutting technology, particularly in achieving high-quality cuts in thicker materials and diminishing gas consumption by increasing gas flow efficiency.

2. Experimental setup & process parameters

The cutting experiments were performed using a disk laser with a wavelength of 1030 nm and an output power of 6 kW to cut 6 mm thick stainless steel (1.4301) samples with a maximum surface roughness of Ra = 0.2 µm. A Precitec HPSSL cutting head was used, and the fiber-guided laser beam ($\varnothing$ = 100 µm) was collimated and focused with focal lengths of 100 mm and 200 mm, respectively. This configuration results in a focal diameter of 200 µm.

The initial approach in the experiments was to determine the optimal cutting speed for minimal burr adhesion, using a standard set of parameters. Burr formation is significantly influenced by cutting speed, where a minimal burr occurs within a narrow optimal range and increases as the speed approaches the maximum cutting speed [12,13]. The maximum cutting speed is reached when the volume of molten and expelled material per unit of time is insufficient to create a kerf, and its onset is characterized by significant changes in the geometry of the cutting front [14]. For this investigation, a standard conical nozzle with the same outlet orifice diameter of 3 mm (StandardØ3) as the cutting whistle (Fig. 3(a)) was employed. The focus position was set 3 mm bellow the sheet surface to create a kerf width of 450 µm. A standoff distance of 0.7 mm and a nitrogen gas pressure of 20 bar were selected. The cutting speed was gradually increased from 4.5 m/min up to the loss of cut. The cutting speed of 5.0 m/min was chosen based on the minimum burr adhesion for this specific parameter set, which is in this case less than 50 µm, Fig. 1.

Although the importance of the standoff distance to the laser cutting process has been well investigated [15–17], small distances below 1 mm, which are commonly used in industrial applications, have often been neglected. Furthermore, the influence of standoff distance on the gas flow oscillation developed by the cutting whistle is yet to be investigated. Therefore, in the following chapters, the standoff distance in the range of 0.3 to 1.1 mm (interval of 0.2 mm) is compared and its influence on the melt flow and the resulting cut quality is evaluated. This will provide a comprehensive understanding of the critical parameters that govern the effectiveness of the cutting whistle in practical applications.

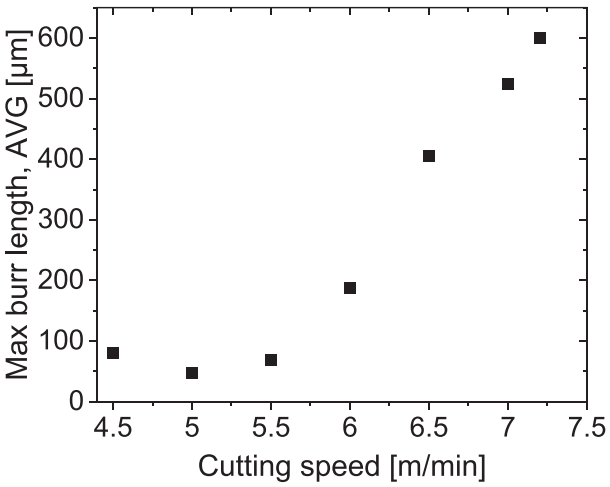

Fig. 1. Dependence of the burr length on the cutting speed.

3. Gas flow diagnostics

Gas flow effects on the cutting process were analyzed using a frozen kerf emulating the cutting process gas flow. The frozen kerf was created with the parameters listed in Table 1. In the experiments, nitrogen gas was regulated to 20 bar, and volume flow was measured by a thermal sensor before reaching the cutting head. To investigate the oscillatory behavior of the gas flowing through the frozen kerf, the associated pressure waves were detected with a microphone below the kerf, as shown in Fig. 2.

The nozzles investigated in the present study are shown in Fig. 3(a). On the left is the standard nozzle for reference and on the right is the cutting whistle. The key geometric features of the cutting whistle include the diameter of the upstream orifice of 4 mm, the cavity length of 3 mm, the cavity diameter of 12.5 mm, and the diameter of the downstream orifice of 3 mm. Both nozzles deliver the same volume flow at the same gas pressure, ensuring an objective performance comparison, as shown in Fig. 3(b). The standoff distance significantly influences volume flow, especially at short distances due to strong obstruction of the gas by the sheet surface. The volume flow increases by 36 % when the standoff is increased from 0.3 to 0.5 mm, the increase is halved with a further increment to 0.7 mm, and from then on, the volume flow reaches a certain plateau with a total increase of only 6 % up to 1250 l/min.

Based on previous investigations, the gas flow rate out of the nozzle is divided into two components: the radial flow into the gap between the nozzle and the sheet surface, and the flow into the kerf. The proportionality between the volume flow rate Q and the cross-sectional area through which the gas flows is expressed in Eqs. (1) and (2). Here, A_{nozzle}, A_{gap} and A_{kerf} represent the areas of the nozzle exit, the gas outer layer in the gap between the nozzle and the sheet surface (illustrated in Fig. 2), and the kerf aperture, respectively.

$$Q \propto A \tag{1}$$

$$A_{nozzle} = A_{gap} + A_{kerf} \tag{2}$$

The cross-sectional areas are given by:

$$A_{gap} = 2\pi \frac{N_d}{2} N_z; A_{nozzle} = \pi \frac{{N_d}^2}{4}; A_{kerf} \approx \frac{N_d}{2} W_K \tag{3}$$

Solving Eqs. (2) and (3) using the nozzle outlet diameter N_d of 3.00 mm and the kerf width W_K of 0.45 mm yields a critical standoff distance N_z^* of 0.68 mm, as given in Eq. (4).

Table 1
Reference process parameters.

Parameter	Unit	Value
Laser power	[kW]	6
Fiber diameter	[µm]	100
Focal length collimator	[mm]	100
Focal length optics	[mm]	200
Focal position	[mm]	−3
Nozzle diameter	[mm]	3
Gas pressure (N_2)	[bar]	20
Standoff distance	[mm]	0.7
Cutting speed	[m/min]	5

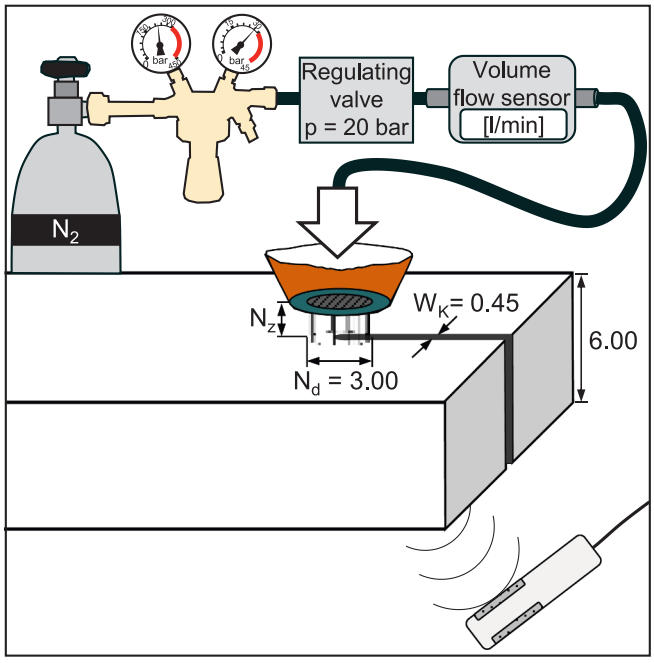

Fig. 2. Sketch of the setup for gas flow diagnostics with indication of the key geometric features for the analysis.

$$N_z^* = \frac{N_d}{4} - \frac{W_K}{2\pi} = 0.68 \tag{4}$$

If the right side of Eq. (2) is larger than the left side, the flow experiences excessive blockage. This occurs when the nozzle distance is less than 0.68 mm, which explain the steep reduction in volume flow rate observed below this nozzle distance.

The importance of the critical standoff distance becomes even clearer when analyzing the acoustic emissions from the gas flow, revealing its direct influence on the oscillation behavior. The acoustic signal was transformed into a frequency spectrum using a Fast Fourier Transform (FFT). The frequency spectra for both nozzles are shown in Fig. 3(c). The spectra of both nozzles have an almost identical shape, except for the resonance frequency peaks observed with the cutting whistle. Above the critical standoff distance, the fundamental frequency is 15 kHz, featuring two higher harmonics. However, when $N_z < N_z^*$, the fundamental frequency and its harmonics are reduced. Specifically, the fundamental frequency drops to 12 kHz when $N_z = 0.5$ mm and to 7 kHz when $N_z = 0.3$ mm.

The underlying resonance mechanism developed by the cutting whistle was discussed in detail in a previous study [11] supported by schlieren and acoustic diagnostics. This study elucidates that a 15 kHz oscillation is generated in the gas flow as a result of a radial feedback loop in the nozzle cavity. The oscillation frequency f for the different harmonic numbers n in this mode was estimated employing Eq. (5) based on a model developed by Rossiter [18]. This frequency depends on the cavity radius R_{cav}, the convection velocity of the generated vortical structure U_c and the sound velocity in the cavity a_{cav}, assumed to be of nitrogen at atmospheric conditions. The equation is expressed as:

$$f = \frac{n}{\left(\frac{R_{cav}}{U_c} + \frac{R_{cav}}{a_{cav}}\right)} \tag{5}$$

Based on Eq. (5), the reduction of the oscillation frequency observed when $N_z < N_z^*$ is caused by a decrease in the convection velocity of the vortical structures within the cavity. Since U_c is related to the free stream velocity U_∞ (conventionally considered $U_c = 0.57U_\infty$) [18–20] and U_∞ is proportional to the volume flow, significant fluctuations in the volume flow, such as occur in the gas obstruction when $N_z < N_z^*$, have an effect on the resulting oscillation frequency. Fig. 4 illustrates the oscillation frequency as function of U_c. Compared to $U_c = 130$ m/s (for $n = 1$) when $N_z > N_z^*$, U_c is reduced to 95 m/s for $N_z = 0.5$ mm and 50 m/s for $N_z = 0.3$ mm.

4. Melt flow diagnostics

A high-speed camera (Photron SA 5) was employed to perform a spatially and temporally resolved diagnosis of the melt flow dynamics on the cutting front. The camera's observation direction was aligned

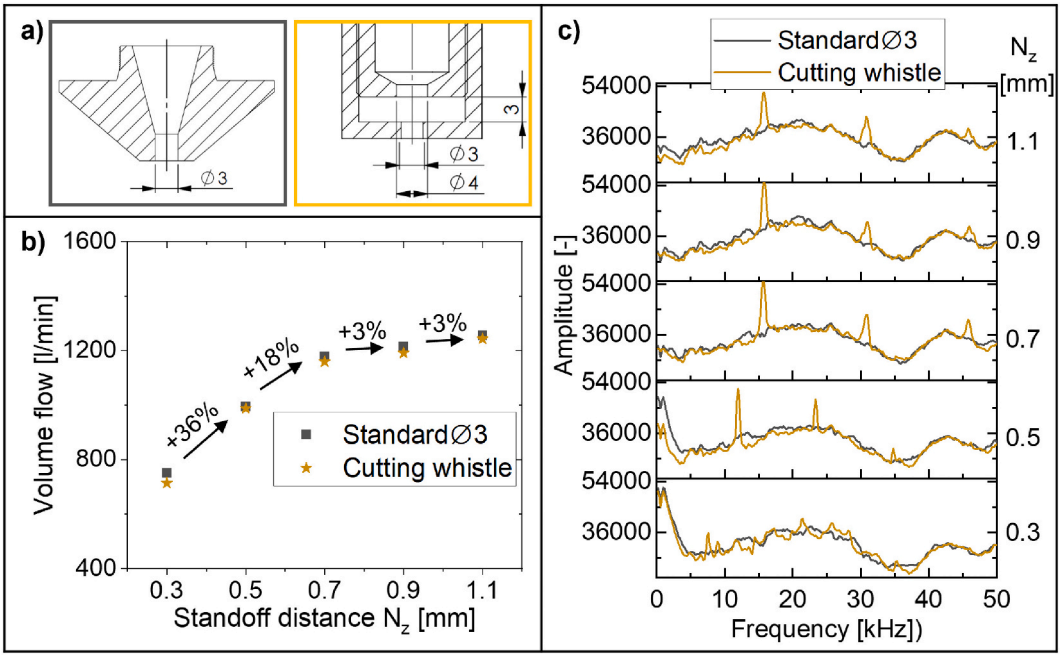

Fig. 3. (a) Drawing of the investigated nozzles (left: standard nozzle; right: cutting whistle); (b) Volume flow rate as function of the nozzle and standoff distance (p = 20 bar); (c) Detected acoustic frequency spectra using the investigated nozzles and standoff distances (p = 20 bar).

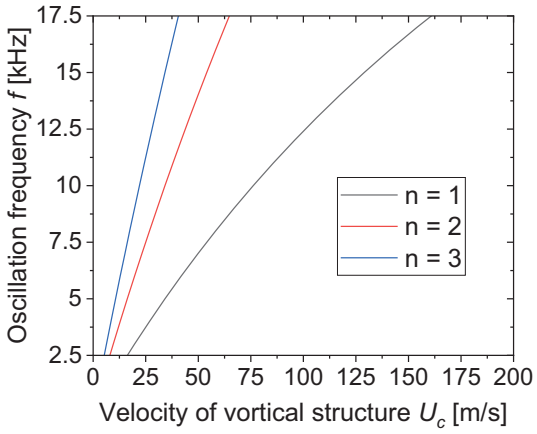

Fig. 4. Oscillation frequency as a function of convection velocity of the vortical structures.

horizontally through the developing kerf in the cutting direction, as shown in Fig. 5(a). The frame rate for the videos was set to 162,750 frames per second, and a spatial resolution of 22 µm/px was achieved using a macro lens with a focal length of 200 mm. The resulting monochrome images have a resolution of 18 px × 276 px (0.4 mm × 6.0 mm) and depict a centered cutting front, as illustrated in Fig. 5(b). Additionally, a short-pass filter was utilized to block emissions with wavelengths above 1000 nm and the associated reflections of the laser beam, ensuring that primarily the thermal emissions from the cutting front were detected. This setup allows for the visualization of the formation of melt waves and their temporal development downstream, as indicated by the brightly glowing spots in the video.

The oscillation behavior of the melt flow was investigated in the frequency domain. For this purpose, an FFT was applied to the temporal fluctuation of the gray values to extract a frequency spectrum for each individual pixel. The highest peak of the resulting frequency spectrum represents the locally dominant oscillation frequency, Fig. 5(c). The spatial distribution of these frequencies and the corresponding amplitudes are presented in color diagrams, Fig. 6.

The use of the standard nozzle resulted in a characteristic melt flow with low frequency (5–10 kHz) melt waves at the upper section of the cutting front, regardless of standoff distance. When a cutting depth of about −1.5 mm is reached, the frequency rapidly rises to its maximum of about 27–32 kHz, as presented in previous studies [9,10]. This frequency is maintained in a very short section of less than half a millimeter. The frequency then gradually reduces downstream towards the exit of the kerf.

The gas flow oscillation developed by the cutting whistle has a strong impact on the melt flow. In agreement with chapter 3, the standoff distance influences the resulting oscillation frequencies. The exact fundamental frequencies detected with the microphone (Fig. 3(c)) are also visualized in the melt flow using the high-speed camera.

At a short standoff distance of 0.3 mm, the fundamental oscillation frequency of 7 kHz is only developed in the upper 2 mm of the melt flow, with a particularly high amplitude in the upper 1 mm. Increasing the standoff distance to 0.5 mm induces a fundamental oscillation frequency of 12 kHz throughout virtually the entire melt flow, with especially high amplitudes in the upper and central sections. Further increasing the standoff to 0.7 mm, i.e., $N_z > N_z^*$, causes most of the melt to exhibit the designed oscillation frequency of 15 kHz, with particularly high amplitudes at the very top, at a cutting depth of −2 mm, −3 mm, and near the kerf exit.

Using larger standoff distances of 0.9 mm and 1.1 mm provides a similar result to 0.7 mm, albeit with slightly lower oscillation amplitudes. Increasing the standoff beyond the critical value increases the area of the gas outer layer (A_{gap}) resulting in a larger percentage of the gas flowing laterally and less gas entering the kerf. Conversely, the gas flow experiences strong obstruction, reducing the volume flow, if $N_z < N_z^*$, as discussed in chapter 3. Thus, a reasonable standoff distance for generating gas flow oscillations coupling most effective to the melt flow is at the critical value.

5. Cut flank quality

The cut flanks were evaluated using an optical profilometer capturing full surface data across the surface with a resolution of 0.1 µm. The quality was quantitatively evaluated using the average surface roughness Rz in accordance with the ISO 9013:2017 standard. The variation of the Rz value across the cutting depth was determined to enable a detailed analysis of the influence of the melt flow dynamics on the surface roughness. For this purpose, the Rz value was extracted from the surface data in short steps of 0.5 mm from top to bottom, and the results are shown in Fig. 7.

The cut flanks produced with the standard nozzle can generally be divided into three zones from top to bottom, irrespective of the standoff distance used. These zones are characterized as follows:

1. Upper section (Z1): This zone exhibits notably high roughness near the top surface, with Rz values ranging between 45 and 60 µm at a cutting depth of −0.5 mm.

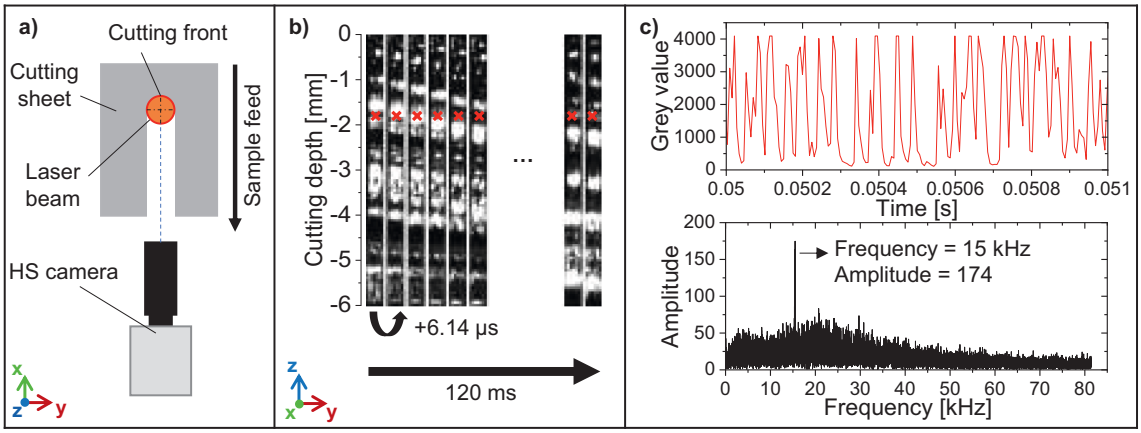

Fig. 5. (a) Sketch of the cutting process from the top view indicating the direction of observation of the camera; (b) Example of a produced time sequence of images of the cutting front; (c) Analysis for the pixel marked in red in (b). (For interpretation of the references to color in this figure legend, the reader is referred to the web version of this article.)

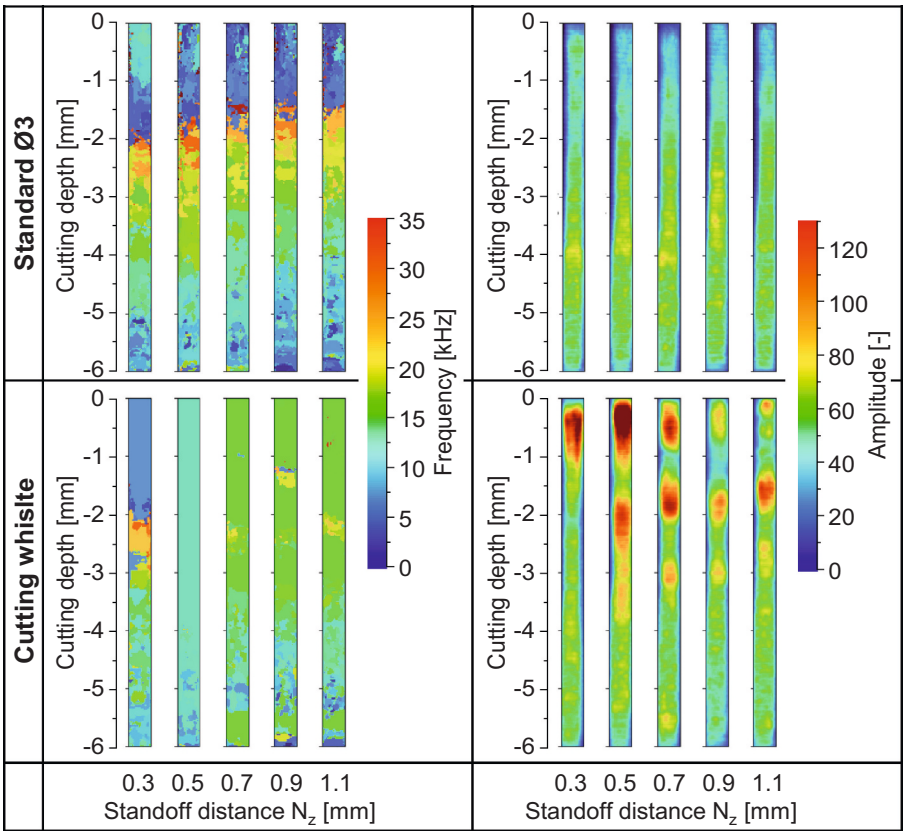

Fig. 6. Overview of the spatial distribution of the dominant frequencies and corresponding amplitudes for standard and cutting whistle nozzles and standoff distances.

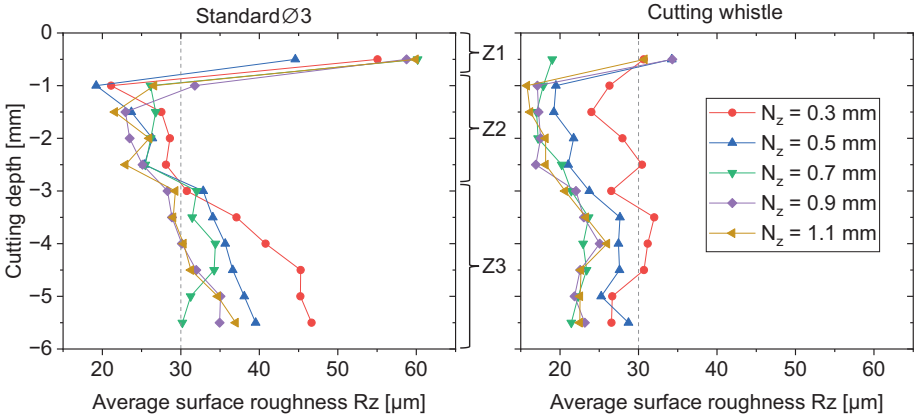

Fig. 7. Average surface roughness Rz measured at an interval of 0.5 mm for different nozzles and standoff distances.

2. Mid-section (Z2): This intermediate zone, spanning from a cutting depth of −1 mm to −2.5 mm, presents the lowest Rz values, typically below 30 µm.
3. Lower section (Z3): The lowest half of the cut flank, representing the third zone, shows high Rz values above 30 µm. The roughness is particularly high when the standoff distance N_z is less than the critical value N_z^*.

The cutting whistle demonstrates a clear reduction in roughness compared to the standard nozzle, with most of the measured Rz values falling below 30 µm. Notably, the Rz values in zones Z1 and Z2 are significantly reduced, making these zones almost indistinguishable in some cases if only the Rz is considered.

The importance of maintaining the critical distance for optimal results regarding the surface roughness is also evident with the cutting whistle. When N_z is less than N_z^*, virtually the entire cutting flank exhibits higher Rz values than when N_z is greater than N_z^*. The best results in terms of surface roughness are obtained for cut flanks with N_z greater than N_z^*, featuring consistently low Rz values of around 20 µm, with the exception of the −0.5 mm cut depth, where the two larger standoff distances yield Rz values of around 30 µm.

This supports the assertion that the optimal standoff distance for effective gas flow coupling in the kerf, and thus a more stable melt flow, is at the critical value. Although the larger standoff distances also provided excellent results, adhering to the critical distance ensures the best surface finish.

Cut flanks are analyzed qualitatively using 3D surface images resulting from the measurements with the optical profilometer, as shown in Fig. 8. These images, color-coded to represent height, depict the flank profiles and striation patterns. For the standard nozzle, pronounced coarse striations near the upper surface lead to the peak Rz value in Z1. The mid-section is characterized by the increase of the flank height up to the maximum at the midpoint of the cut depth, i.e., the narrowest section of the kerf, indicating a convergent kerf profile. The striations are slightly tilted backwards and the frequency of striations decreases, as some striations from the upper section are apparently merged at this point and also featuring the lowest Rz values. The lower section is characterized by a stochastic variation in kerf profile, with striations frequently maintaining the height from the mid-section, alternating with deep local kerf widening indicated by the blue areas increasing the Rz values.

While the cutting whistle has no significant influence on the kerf profile compared to the standard nozzle, it creates a distinctly different striation pattern. In the upper section, the coarse structures are not developed, resulting in a finer surface. In the mid-section, there is a noticeable reduction in the height variation of the striations. The lower section exhibits a more stable divergent kerf profile, with less stochastic variation in kerf profile than for the standard nozzle, leading to a decrease in roughness as reflected in the Rz values.

6. Discussion

The two sections with higher Rz values using the standard nozzle, specifically Z1 and Z3, are primarily characterized by frequencies in the lower range of about 5–10 kHz, as indicated by the blue shades in the frequency color diagrams, Fig. 10. In Z1, the low frequency upstream in the melt flow indicates the time required for the melt waves to form and grow before reaching a threshold value that allows them to detach and start moving downstream, resulting in irregular melt flow in this region. This is particularly evident in the streak images of the cutting front apex (Fig. 9) where the melt waves are recognizable by the white stripes, revealing intermittent pauses of up to 0.2 ms at the top of the image, corresponding to a frequency of about 5 kHz.

Across Z3, from top to bottom, the frequency of about 15 kHz (Fig. 10, green color) decreases by a factor of three, indicating the range in which melting instabilities are more pronounced. These can be identified by the larger dark areas in the streak images, which are followed by large melt accumulations, shown by the dotted lines in Fig. 10. The significance of this phenomenon is highlighted by the local maximum amplitude in the color diagram. These accumulations result from interactions between melt waves, mediated by surface tension as the melt flows downstream [4].

In contrast, the cutting whistle creates a more uniform melt flow that begins at the top of the cutting front, where time required for the waves to flow downstream is determined by the oscillation frequency (Fig. 9). Synchronized oscillating waves at a frequency of 15 kHz flow downstream without forming large accumulations, as indicated by the arrows in Fig. 10. This improvement is explained by the balance between the gas force and the resistive surface tension that governs the melt flow. The oscillation of the gas flow in the kerf causes variations in local gas velocity and pressure gradients. Since the shear stress exerted by the gas on the melt stream is directly proportional to the gas flow [2], oscillations in gas velocity cause the shear stress to oscillate at the same frequency. This behavior directly counteracts the resistive surface tension, allowing the threshold for the detachment of melt accumulations to be reached faster, resulting in smaller accumulations and locally lower roughness depth. The regular melt wave pattern on the cutting front not only indicates a more efficient melt ejection mechanism but also affects the formation of the lateral cutting flanks due to regular multiple reflections [8]. Consequently, the cutting whistle provides a significant advantage by ensuring a more consistent and efficient melt ejection, leading to improved surface quality.

7. Conclusion & further outlook

This study investigates the impact of using a cutting whistle on melt flow and surface roughness during laser fusion cutting of 6 mm thick stainless steel sheets, comparing its performance to that of a standard conical nozzle. The research focuses on the influence of gas flow oscillations on melt flow, the effect of standoff distance on gas flow coupling in the kerf, and the potential of enhanced oscillatory gas flow behavior to stabilize melt flow at the lower cutting front.

The findings reveal that the oscillatory behavior of gas flow induced by the cutting whistle plays a crucial role in achieving lower surface roughness by promoting faster detachment of melt accumulations, enhancing melt ejection, and minimizing the formation of coarse striations. Roughness is particularly low if the frequency is homogeneously distributed over the cutting front and there is sufficient amplitude for coupling to the melt waves. The oscillation frequency is primarily determined by the configuration of the resonant nozzle cavity, while the correct standoff distance is critical for the coupling the oscillating gas flow in the cutting kerf and therefore generating this oscillation in the melt flow across the cutting front. An optimal standoff distance was determined, based on the geometrical features constraining the gas flow. Maintaining this standoff distance is essential for increasing melt flow stability and reducing surface roughness. Using a standoff distance

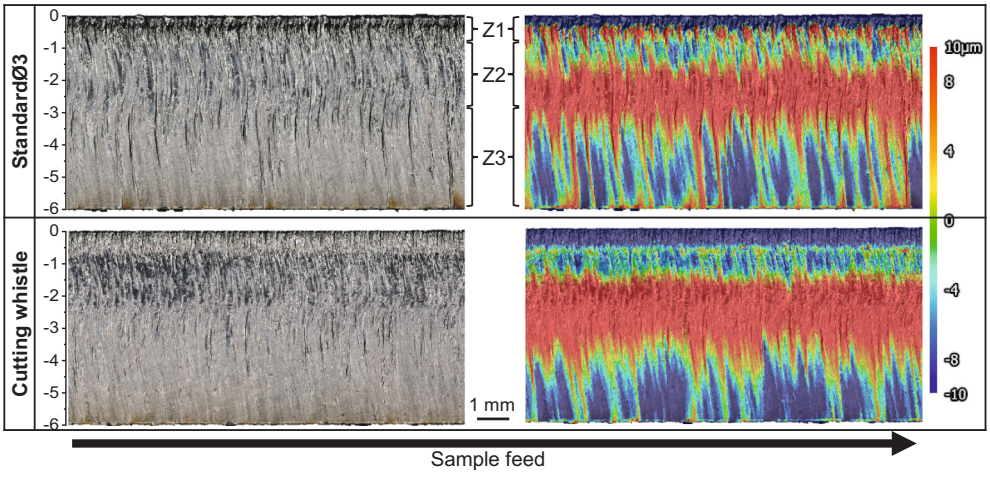

Fig. 8. 3D images of the cut flanks (N_z = 0.7 mm).

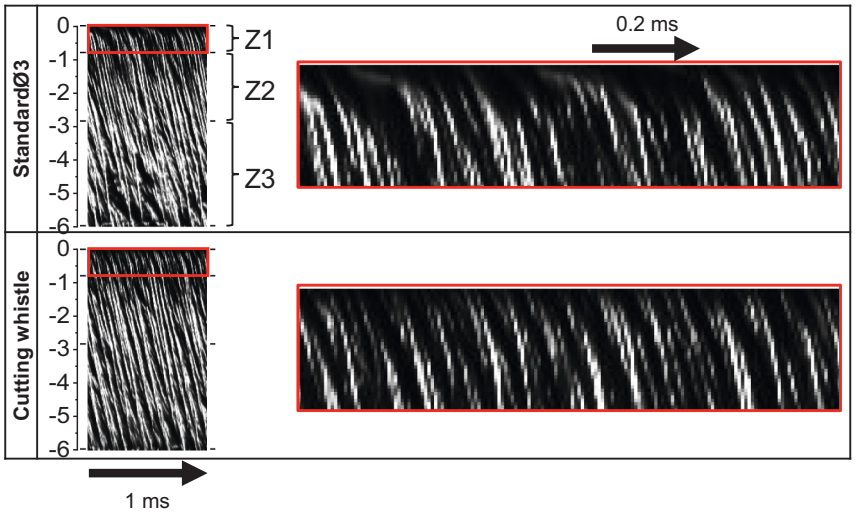

Fig. 9. Streak images of the cutting front apex (N_z = 0.7 mm).

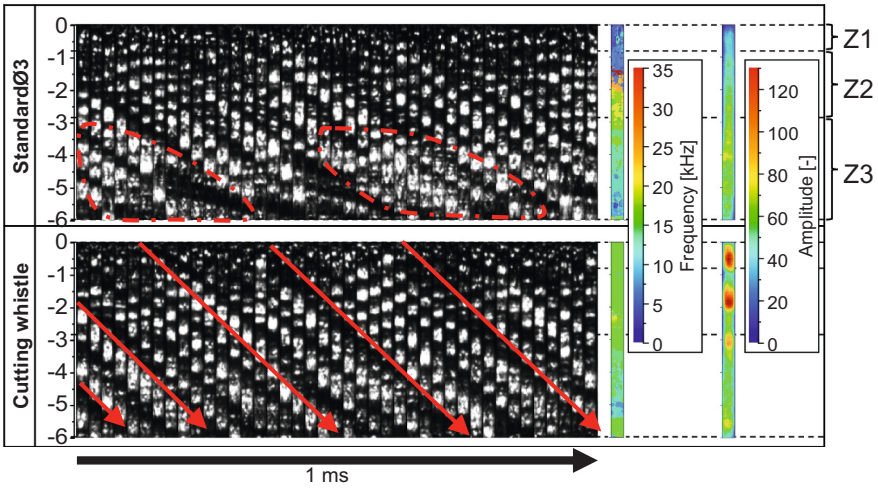

Fig. 10. Image sequences of the cutting front (N_z = 0.7 mm) and corresponding frequency distribution and amplitudes.

below the critical value diminishes gas volume flow and therefore the oscillation frequency generated by the cutting whistle. Performance evaluations show that the cutting whistle provides higher robustness regarding surface roughness compared to a standard conical nozzle, consistently reducing the Rz value in the upper 1 mm and lower half of the cut flanks, regardless of the standoff distance. Under optimal conditions, it reduces the Rz values across the entire cutting depth by approximately 35 % and prevents coarse structures near the upper sheet surface and at the bottom.

The promising results of this study open several avenues for future research and development. Utilizing advanced diagnostics as X-ray imaging with synchrotron radiation to analyze melt flow dynamics from a lateral perspective relative to cutting direction can provide more insights into the interaction between gas flow oscillations and melt behavior. This could support the development of models to predict and control melt flow and surface quality. Material-specific studies are also crucial. Expanding the scope of this research to include a across different materials, such as different metals and alloys, and thicknesses could provide a deeper understanding of the optimal conditions for diverse cutting applications. Finally, implement and test the cutting whistle in manufacturing environment can validate the laboratory findings and address any practical challenges, paving the way for widespread adoption in the laser cutting industry. By continuing to explore and refine the technology behind the cutting whistle, significant advancements in laser cutting processes can be achieved, leading to improved efficiency, quality, and applicability across various industrial sectors.

CRediT authorship contribution statement

M. de Oliveira Lopes: Writing – original draft, Validation, Methodology, Investigation, Formal analysis, Data curation, Conceptualization. **F. Schneider:** Writing – review & editing. **A. Gillner:** Writing – review & editing, Supervision, Project administration. **C. Häfner:** Supervision.

Declaration of competing interest

The authors declare that they have no known competing financial interests or personal relationships that could have appeared to influence the work reported in this paper.

Acknowledgements

The presented investigations were carried out at the Chair of Laser Technology LLT of RWTH Aachen University and Fraunhofer Institute for Laser Technology ILT within the framework of the collaborative

Research Centre SFB1120-236616214 “Bauteilpräzision durch Beherrschung von Schmelze und Erstarrung in Produktionsprozessen” and funded by the Deutsche Forschungsgemeinschaft e.V. (DFG, German Research Foundation). The sponsorship and support are gratefully acknowledged.

References

[1] Belforte David A. The global market for industrial laser processing. In: PhotonicsViews. 17 (2); 2020. S. 35–37. https://doi.org/10.1002/phvs.202070211.
[2] Petring D. Anwendungsorientierte Modellierung des Laserstrahlschneidens zur rechnergestützten Prozeßoptimierung: Zugl.: Aachen, Techn. Hochsch., Diss.: 1995 (Berichte aus der Lasertechnik). Aachen: Shaker. 1995.
[3] Vicanek M, Simon G, Urbassek HM, Decker I. Hydrodynamical instability of melt flow in laser cutting. J Phys D Appl Phys 1987;20(1):140–5. https://doi.org/10.1088/0022-3727/20/1/021.
[4] Hirano Koji, Fabbro Remy. Experimental investigation of hydrodynamics of melt layer during laser cutting of steel. J Phys D Appl Phys 2011;44(10):S. 105502. https://doi.org/10.1088/0022-3727/44/10/105502.
[5] Arntz D, Petring D, Stoyanov S, Jansen U, Schneider F, Poprawe R. In situ visualization of multiple reflections on the cut flank during laser cutting with 1 μ m wavelength. J Laser Appl 2018;30(3):032206. https://doi.org/10.2351/1.5040614.
[6] Petring D, Arntz A, Stoyanov S, Schneider F. Effects of Beam Power and Power Density Distribution on Process and Quality Issues during Fiber Laser Cutting of Stainless Steel Sheet Metal. In: Lasers in Manufacturing 2019: Munich ICM, Internationales Congress Center München, Germany, June 24–27; 2019.
[7] Arntz A, Petring D, Schneider F, Stoyanov S, Halm U, Gillner A. Quantitative Analysis of the Temporal Distance between Melt Waves on the Cutting Front Apex during Laser Fusion Cutting of Stainless-Steel Sheet Metal with 1 Micron Wavelength. In: Lasers in Manufacturing 2019: Munich ICM, Internationales Congress Center München, Germany, June 24–27; 2019.
[8] Petring Dirk, Molitor Thomas, Schneider Frank, Wolf Norbert. Diagnostics, Modeling and Simulation: Three Keys Towards Mastering the Cutting Process with Fiber, Disk and Diode Lasers. Physics Procedia 2012;39:S. 186–196. https://doi.org/10.1016/j.phpro.2012.10.029.
[9] Arntz D, Petring D, Schneider F, Poprawe R. In situ high speed diagnosis—A quantitative analysis of melt flow dynamics inside cutting kerfs during laser fusion cutting with 1 μ m wavelength. J Laser Appl 2019;31(2):022206. https://doi.org/10.2351/1.5096091.
[10] Arntz-Schroeder Dennis, Petring Dirk. Analyzing the Dynamics of the Laser Beam Cutting Process. PhotonicsViews 2020;17(2):S. 43–47. https://doi.org/10.1002/phvs.202000015.
[11] de Oliveira Lopes M, Petring D, Stoyanov S, Gillner A. Control of melt dynamics in laser cutting based on a resonant nozzle cavity. J Manuf Process 2023;105:S. 399–406. https://doi.org/10.1016/j.jmapro.2023.09.051.
[12] Stoyanov S, Petring D, Piedboeuf F, Lopes M, Schneider F. Numerical and experimental investigation of the melt removal mechanism and burr formation during laser cutting of metals. J Laser Appl 2023;35(4):042028. https://doi.org/10.2351/7.0001182.
[13] Mahrle Achim, Borkmann Madlen, Pfohl Peer. Factorial Analysis of Fiber Laser Fusion Cutting of AISI 304 Stainless Steel: Evaluation of Effects on Process Performance, Kerf Geometry and Cut Edge Roughness. In: Materials (Basel, Switzerland); 2021. https://doi.org/10.3390/ma14102669. 14 (10).
[14] Lind Jannik, Fetzer Florian, Hagenlocher Christian, Blazquez-Sanchez David, Weber Rudolf, Graf Thomas. Transition from Stable Laser Fusion Cutting Conditions to Incomplete Cutting Analyzed with High-speed X-ray Imaging. J Manuf Process 2020;60:470–80. https://doi.org/10.1016/j.jmapro.2020.10.068.
[15] Zefferer H, Petring D, Beyer E. Investigations of the gas flow in laser beam cutting. In: Proceedings of the 3rd Int. Beam Technology Conference Karlsruhe (Germany, March 13–14) 210–4; 1991.
[16] Man HC, Duan J, Yue TM. Analysis of the dynamic characteristics of gas flow inside a laser cut kerf under high cut-assist gas pressure. J Phys D Appl Phys 1999;32(13):S. 1469–1477. https://doi.org/10.1088/0022-3727/32/13/306.
[17] Chen Kai, Lawrence Yao Y, Modi Vijay. Gas Dynamic Effects on Laser Cut Quality. J Manuf Process 2001;3(1):S. 38–49. https://doi.org/10.1016/S1526-6125(01)70032-1.
[18] Rossiter, J. E.: Wind tunnel experiments on the flow over rectangular cavities at subsonic and transonic speeds. In: London: Aeronautical Research Council, Reports and Memoranda, Rept. 3488. URL: https://reports.aerade.cranfield.ac.uk/handle/1826.2/4020.
[19] Heller HH, Holmes DG, Covert EE. Flow-induced pressure oscillations in shallow cavities. J Sound Vib 1971;18(4):S. 545–553. https://doi.org/10.1016/0022-460X(71)90105-2.
[20] Handa Taro, Urita Akira. Experimental study of small supersonic circular jets actuated by a cavity. Experimental Thermal and Fluid Science 2018;96:S. 419–429. https://doi.org/10.1016/j.expthermflusci.2018.03.031.